

## Wideband and 2D vibration energy harvester using multiple magnetoelectric transducers

Jin Yang\*, Qiangmo Yu, Jiangxin Zhao, Nian Zhao, Yumei Wen and Ping Li

*Department of Optoelectronic Engineering, Research Center of Sensors and Instruments, Chongqing, China*

*(Received March 11, 2014, Revised November 17, 2014, Accepted January 9, 2015)*

**Abstract.** This paper investigates a magnetoelectric (ME) vibration energy harvester that can scavenge energy in arbitrary directions in a plane as well as wide working bandwidth. In this harvester, a circular cross-section cantilever rod is adopted to extract the external vibration energy due to the capability of its free end oscillating in arbitrary in-plane directions. And permanent magnets are fixed to the free end of the cantilever rod, causing it to experience a non-linear force as it moves with respect to stationary ME transducers and magnets. The magnetically coupled cantilever rod exhibits a nonlinear and two-mode motion, and responds to vibration over a much broader frequency range than a standard cantilever. The effects of the magnetic field distribution and the magnetic force on the harvester's voltage response are investigated with the aim to obtain the optimal vibration energy harvesting performances. A prototype harvester was fabricated and experimentally tested, and the experimental results verified that the harvester can extract energy from arbitrary in-plane directions, and had maximum bandwidth of 5.5 Hz, and output power of 0.13 mW at an acceleration of 0.6 g (with  $g=9.8 \text{ ms}^{-2}$ ).

**Keywords:** two-dimensional vibration energy harvesting; nonlinear and two-mode motion; ME transducer; cantilever rod

### 1. Introduction

In the past decade, energy scavenging from ambient vibration sources to electrical energy has attracted a considerable scientific interest, which provides a promising way to replace batteries as a main power source for most small-scale electronic devices (Casciati *et al.* 2012, Kim *et al.* 2013). There are several typical vibration-to-electricity mechanisms, such as piezoelectric (Aladwani *et al.* 2012, Zhu *et al.* 2011), electromagnetic (Arroyo *et al.* 2011, Chen *et al.* 2012), electrostatic (Nguyen *et al.* 2010, Tvedt *et al.* 2010), or ME transduction mechanisms (Wang and Yuan 2008, Yang *et al.* 2011, Yang *et al.* 2011). Recently, in order for these vibration energy harvesters to be effective in widespread applications, many technologies including broadening the frequency range and improving the power density of the harvesters were proposed and shown some promise. For example, monostable duffing, impact, bistable oscillators and multi-mode have been used successfully to broaden the effective operational frequency ranges of the vibration energy harvesters (Aladwani *et al.* 2013, Aldraihem and Baz 2011, Berdy *et al.* 2012, Chen *et al.* 2013,

---

\*Corresponding author, Professor, E-mail: yangjin@cqu.edu.cn

Erturk and Inman 2011, Ferrari *et al.* 2010, Guan *et al.* 2012, Jung *et al.* 2011, Moss *et al.* 2011, Zhang *et al.* 2012). Despite the transduction mechanisms and novel structures, there is still an obstacle facing realistic implementation in most of the vibration-based energy harvester, because they are designed to harvest energy in a single direction of the ambient vibrations. But a vibration source in real environment may exhibit several motion directions over time. Hence, they may not generate power effectively in the case of a motion with multiple or time-variant motion directions.

To address this issue, Scott *et al.* proposed a bi-axial oscillator using a magnet and ball bearing arrangement to extract vibration energy with arbitrary motion directions in a plane (Moss *et al.* 2012). However, the AISI 52100 ball oscillating on the surface of the Terfenol-D will damage the transducer inevitably, and the bandwidth of the harvester was narrow (about 1 Hz). Bartsch reported a two-dimensional electrostatic resonant micro energy generator to extract energy from arbitrary direction motions (Bartsch *et al.* 2009). However, the level of harvested power was too low (1-100pW), and the bandwidth was only 1Hz. Zhu *et al.* devised a 2-DOF (Degree-of-Freedom) MEMS electrostatic harvester, in which a seismic mass is restricted by 16 beams and moves in the X- and Y-axes to absorb energy from the directions of X, Y, and diagonals with resonance frequencies of 38 520 and 38 725 Hz (Zhu *et al.* 2011). But an additional dc bias is needed to be applied to the seismic mass, and a possible application of this harvester is ultrasonic energy harvesting. In low frequency vibration case (<1 kHz), a similar 2-DOF MEMS electrostatic energy harvester for two-axis vibration was reported (Kim and Chun 2012). But the harvester has a limitation of vibration frequency, and should be improved to increase the frequency range.

ME transducers were originally intended for magnetic field sensors but have recently been used in vibration energy harvesting. The ME transducer may be composed of magnetostrictive/piezoelectric laminate composites. Magnetostrictive materials have high energy density and high magnetomechanical coupling effect; thus, ME generators not only have the same advantage of piezoelectric generators but can also produce higher mechanical stress and power output than piezoelectric cantilever beam generators (Wang and Yuan 2008, Yang *et al.* 2011). Therefore, we report on a design for an energy harvester using ME transducers, in which only one vibrating body is used to extract the ambient vibration energy with arbitrary in-plane motion directions, and the frequency bandwidth can be enhanced by nonlinear behavior of the magnetic force.

## 2. Harvester design

The proposed vibration energy harvester is graphically described in Fig. 1. A circular cross-section elastic rod is adopted as the oscillating body, not the traditional thin cantilever beam, and one of its ends is fixed to the harvester frame, and the other end is free and could oscillate with in-plane (y-z plane) arbitrary directions to extract the ambient vibration energy. The ME transducer has a laminate structure made up of two magnetostrictive layers and one piezoelectric layer. And the piezoelectric layer is polarized in its thickness direction, and the magnetostrictive layers are magnetized along the longitudinal direction. The magnetic circuit consists of two sets of magnets. Each set is made of a hollow cylindrical magnet, within which a smaller cylindrical magnet is coaxially mounted. And one set of magnets is fixed at the free end of the elastic rod as the proof mass, and the other set and the four ME transducers are fixed on the harvester frame. The magnets are all axially magnetized, and are configured in opposite polarities arrangement. As the harvester is excited at arbitrary angle of  $\theta$ , the movable magnets will oscillate relatively to the four fixed transducers. As a result, the magnet circuit will produce a concentrated magnetic flux gradient

through the ME transducers, and the magnetic fluxes inside the ME transducers vary. Then the varying magnetic field causes the magnetostrictive layers to generate stress. The stress is then transmitted to the piezoelectric layer, which generates electrical power.

### 3. Harvester analysis

#### 3.1 Voltage output analysis

In this harvester, when the external acceleration causes a relative motion between the fixed ME transducers and the movable magnets, the magnetic flux inside the ME transducer will vary, and there will be electrical power generated due to magnetolectric induction. According to the principle of the ME transducer (Wang and Yuan 2008, Yang *et al.* 2011), the ME voltage output can be expressed as

$$V_{out} = \Delta H \times \alpha_{ME,H_{bias}} \tag{1}$$

where  $\Delta H$  is the magnetic field variation along longitudinal direction (x-axial) induced by the ME transducer, and  $\alpha_{ME,H_{bias}}$  is the ME voltage coefficient under a DC magnetic bias field,  $H_{bias}$ . At low frequency (e.g.,  $f < 1$  kHz or lower),  $\alpha_{ME,H_{bias}}$  is given by (Wang and Yuan 2008, Yang *et al.* 2011)

$$\alpha_{ME,H_{bias}} \approx \frac{n(1-n)t_c d_{33,m,H_{bias}} d_{31,p}}{\epsilon_{33}[n(1-k_{31}^2)s_{11}^E + (1-n)s_{33,H_{bias}}^H]} \tag{2}$$

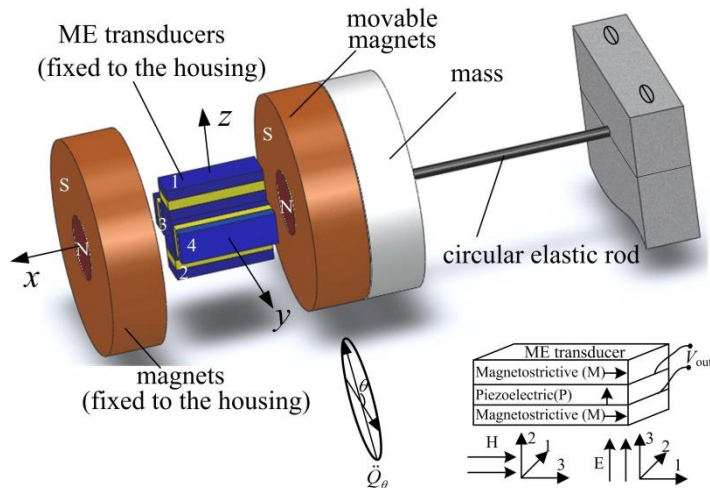


Fig. 1 Schematic design of the vibration energy harvester

where,  $n$  is the thicknesses ratio of the magnetostrictive and piezoelectric layers in the ME transducer.  $t_c$  is the thickness of the transducer.  $d_{33,m,H_{bias}}$  and  $d_{31,p}$  are the piezomagnetic constant and piezoelectric coefficient, respectively.  $s_{11}^E$ ,  $\epsilon_{33}$ ,  $s_{33,H_{bias}}^H$  and  $k_{31}$  are the piezoelectric elastic compliance, permittivity tensor, piezomagnetic elastic compliance, and piezoelectric electromechanical coupling coefficient, respectively. According to Eqs. (1) and (2), the voltage output  $V_{out}$  significantly depends upon the induced magnetic field variation,  $\Delta H$ , and the ME voltage coefficient,  $\alpha_{ME,H_{bias}}$ . In order to achieve high output performance, the ME transducer should work in a better DC magnetic bias field to obtain high ME voltage coefficient  $\alpha_{ME,H_{bias}}$ , and undergo large enough magnetic field variation  $\Delta H$  at a small relative displacement to the movable magnets.

In the magnetic circuit with fixed dimensions, the ME transducers will induce different magnetic fields and variations when placed at different positions relative to the magnetic circuit, because the magnetic field distribution is non-uniform. Therefore, the initial positions of the ME transducers at the static equilibrium are key factors on the output voltage of the harvester. In order to illustrate the effect of the initial position on the ME output voltage, the software of Ansoft's Maxwell 3D is employed to simulate and analyze the magnetic field distribution of the magnetic circuit. In simulation, the axial length of the hollow cylindrical magnet is 5.0 mm, and outer diameter is 20.0 mm, and inner diameter is 6.0 mm. The dimension of the smaller cylindrical magnet is  $\Phi 6.0$  mm $\times$ 5.0 mm. The remnant flux density of the magnets is 1.3 T. The magnetostrictive layers of the ME transducer are designed with dimensions of 12.0 mm $\times$ 3.0 mm $\times$ 1.0 mm, and the relative permeability of the magnetostrictive layers is 5.0. The piezoelectric layer has the dimensions of 12.0 mm $\times$ 3.0 mm $\times$ 0.8 mm. In Fig. 1, the magnetized direction of the magnetostrictive layers is parallel to the x-axis (longitudinal direction of magnetostrictive layer). The x component of the magnetic field is variable along the y- and z- directions due to the non-uniform magnetic field distribution, thus we regard the average magnetic field of the x-direction as the induced magnetic field of the magnetostrictive layers. In this model, the origin of coordinate is established at the central point of the magnetic circuit. The magnetic field distribution  $H(y, z)$  along x-axis, which is the average value in the volume of the ME transducer, is calculated when the movable magnets are set to translate at different positions along y- and z- axes in Fig. 1. Fig. 2(a) plots the simulated magnetic field  $H(y, z)$  and the corresponding variation as a function of the position. The variation is defined as  $\partial H(y, z)/\partial y|_{-20 \leq z \leq 20}$  (or  $\partial H(y, z)/\partial z|_{-20 \leq y \leq 20}$ ). As indicated in Fig. 2, the distributions of the magnetic field and variation are both completely symmetrical. The maximum magnetic field appears in a circle with the radius of 5.0 mm, and the large magnetic field variations are observed in two circles with the radius of 3.0 mm and 11.0 mm, respectively. The values of 3.0 mm and 11.0 mm are close to the radius of the small cylindrical magnet and the hollow cylindrical magnet, respectively. So the four ME transducers should be placed on the two boundaries to induce large magnetic field variations. Furthermore, Fig. 3 plots the magnetic field  $H(0, z)$  and variation  $\partial H(0, z)/\partial z|_{-20 \leq z \leq 20}$  along z-axial. The absolute peak values of the variations reach about 20.0 Oe/mm and 28.0 Oe/mm at  $\pm 3.0$  mm and  $\pm 11.0$  mm. Moreover, the magnetic fields at  $\pm 3.0$  mm are  $\sim 393.0$  Oe, which are closer to the optimal bias magnetic field condition of the ME transducer  $\sim 410.0$  Oe. While the corresponding magnetic fields at  $\pm 11.0$  mm are  $\sim 341.0$  Oe, which are farther from the optimal bias

magnetic field of the ME transducer. Therefore, the common boundary (radius of 3.0 mm) between the hollow cylindrical magnet and the smaller cylindrical magnet should be choose as the initial position to place the ME transducer, because the transducer can work in a better condition of the DC bias field.

When the four ME transducers are placed symmetrically on the common boundary (radius of 3.0 mm) and the movable magnets oscillate along z-axis, the magnetic fields and variations of two adjacent ME transducers are simulated, and the results are shown in Fig. 4. The maximum magnetic variation of the ME transducer 1 (placed at initial position of 3 mm in z-axial) is still 20.0 Oe/mm, while the value of the adjacent ME transducer 3 (placed at initial position of 3 mm in y-axial) is 0.0 Oe/mm. It can be seen that, two adjacent ME transducers induce different magnetic filed variations, which will lead to different output voltages when the movable magnets oscillate along an arbitrary direction.

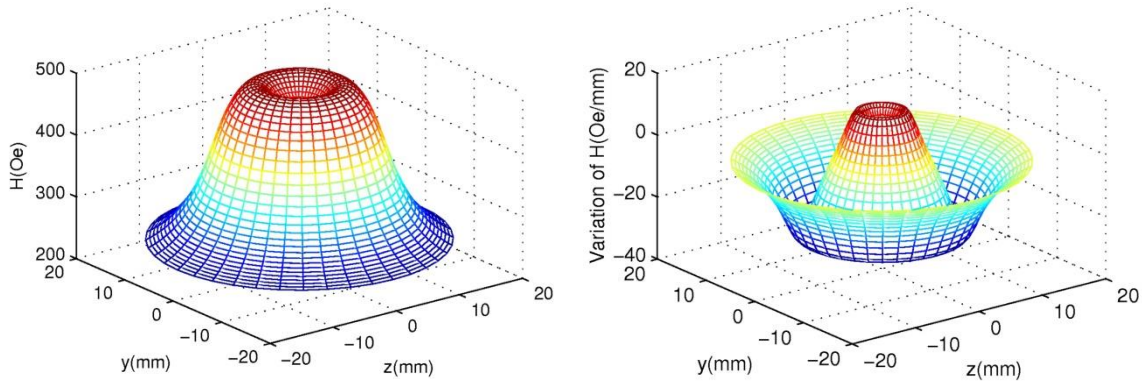


Fig. 2 Magnetic field and variation in the magnetic circuit

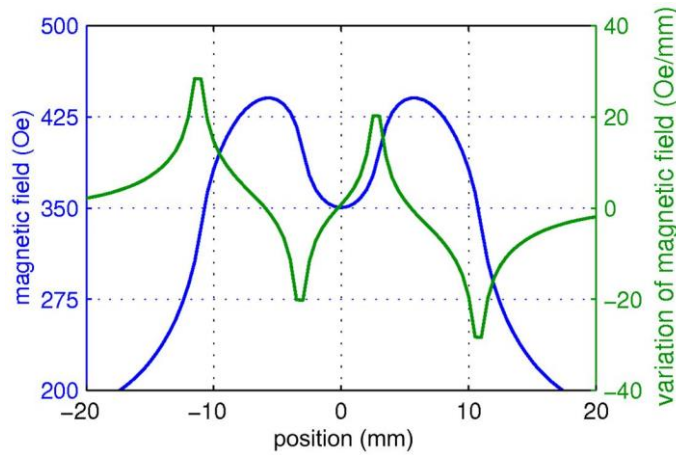


Fig. 3 Magnetic field and variation along z-axial

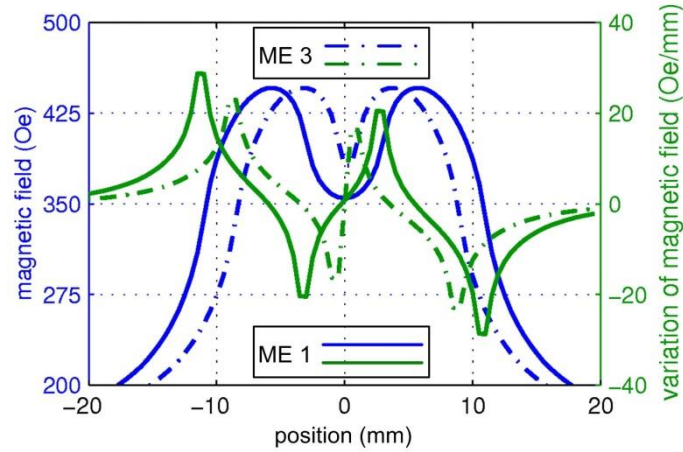


Fig. 4 Magnetic fields and variations of two adjacent ME transducers

### 3.2 Vibration analysis

In the harvester, there exists a magnetic force between the movable magnets and the fixed parts, including the ME transducers and the fixed magnets. In this case, the motion of the elastic rod under an arbitrary excitation direction will be affected by the magnetic force. In this section, the ANSYS software is used to analyze the influence of the magnetic coupling on the motion behavior of the harvester. In the simulation, the circular rod is made up of  $\Phi 1.5 \text{ mm} \times 40.0 \text{ mm}$  high elastic beryllium steel. The proof mass is 20.0 g. And the parameters of the magnetic circuit and the ME transducers are the same as those in Section 3.1. Fig. 5 plots the simulated magnetic force of the elastic rod, and the inset figure shows the z-component of the magnetic force as a function of z displacement. It is clear that the magnetic force is the nonlinear function of the displacement. By nonlinear behavior of the magnetic force, hardening or softening response would occur in frequency response of the harvester, which allows the working bandwidth to be broadened in either direction (Stanton *et al.* 2009, Ramlan *et al.* 2010).

In addition, Fig.6 shows the simulated mode shapes of the rod at the excitation angle of  $45^\circ$  and acceleration of 0.4 g. And a comparison of the motion characteristics of the cantilever rod at different excitation angles is listed in Table 1. For this purpose, the key point was the coupled magnetic force between the movable magnets and the fixed parts. Therefore, the simulated magnetic force in Fig. 5 was used as force input into the ANSYS software, which acted on the cantilever rod with the inertia force due to external acceleration. The result shows that there exist two motion modes (I and II) at each excitation angle. Taking the result at  $45^\circ$  as example, at mode I, the cantilever rod with the movable magnets oscillates along the angle of  $45^\circ$  with the motion amplitude of 6.5 mm, and at mode II, the motion changes to oscillate along  $135^\circ$  with the amplitude of 7.0 mm. It can be seen that, the magnetic coupling results in double-model motion of the rod to exhibit double-power peaks, and this behavior will further increase the bandwidth of the harvester in arbitrary excitation directions.

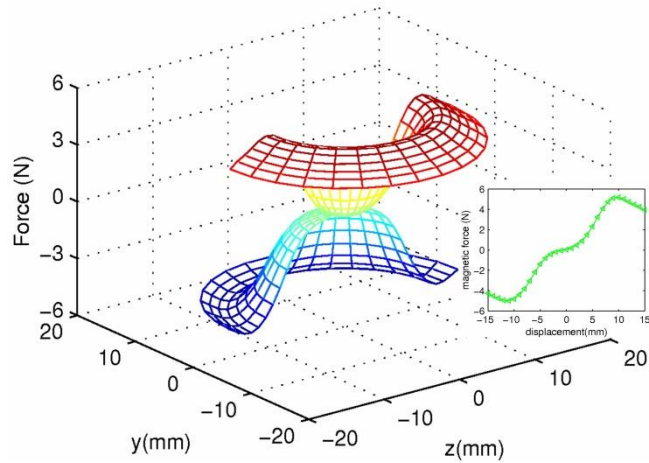


Fig. 5 Simulated magnetic force

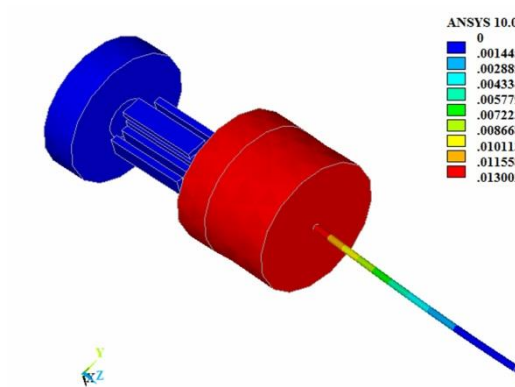


Fig. 6 Mode shapes of the rod at the excitation angle of 45° and acceleration of 0.4 g

Table 1 Comparison of the motion characteristics of the cantilever rod at different excitation angles (PP: peak-peak motion amplitude)

	Mode I, PP (mm)	Mode II, PP (mm)
0°	7.0 (along 0°)	7.2 (along 90°)
45°	6.5 (along 45°)	7.0 (along 135°)
90°	7.4 (along 90°)	8.0 (along 0°)

## 4. Experiment and results

### 4.1 Experimental setup

A prototype of the harvester is devised to validate the design and analysis of the vibration energy harvesting. The circular rod is made up of  $\Phi 1.5 \text{ mm} \times 40 \text{ mm}$  high elastic beryllium steel. The proof mass weighs 20.0 g. To fabricate the ME transducer, PZT-5H (commercially available from No. 26 Research Institute, China) and Terfenol-D (commercially available from Gansu Tianxing, China) are selected as the piezoelectric phase and the piezomagnetic phase, respectively.  $d_{33,m}$ ,  $s_{33}^H$  and  $\mu_r$  of Terfenol-D are  $7.6 \times 10^{-9} \text{ m/A}$ ,  $40 \times 10^{-12} \text{ m}^2/\text{N}$  and 5, respectively.  $d_{31,p}$ ,  $s_{11}^E$ ,  $\varepsilon_{33}$  and  $k_{31}$  are  $-270 \text{ p C/N}$ ,  $14.8 \text{ m}^2/\text{N}$ , 3800 and 0.38, respectively. One PZT-5H layer is bonded between two Terfenol-D layers using epoxy adhesive with curing temperature of  $80^\circ\text{C}$  for 1 h to make the ME laminate composite. The Terfenol-D layers are designed with dimensions of  $12.0 \text{ mm} \times 3.0 \text{ mm} \times 1.0 \text{ mm}$ , and the PZT-5H layer has the dimensions of  $12.0 \text{ mm} \times 3.0 \text{ mm} \times 0.8 \text{ mm}$ . Lead wires are soldered from the two metallic electrodes of the piezoelectric layer for electrical output. The dimensions and the magnetic parameters of the magnets in magnetic circuit are the same as these in Section 3.1.

The experiment set up is illustrated in Fig. 7. The prototype is mounted on an electrodynamic shaker (Bruel and Kjaer) powered by an amplified sinusoidal wave from a function generator (Stanford DS345) and an amplifier (LabworkPa-13). An accelerometer is mounted on the vibration shaker table, which is connected to a shaker controller to measure and control the amplitude of the acceleration applied to the prototype. The lead wires from the ME transducer are connected to a digital oscilloscope (Tektronix TDS2022B) to measure and store the output voltage of the prototype. In all measurements, a mechanical structure is used to alter the exciting angle  $\theta$ , and the output voltages at excitation frequencies of 5 to 50 Hz were recorded for different y-z plane excitation angles.

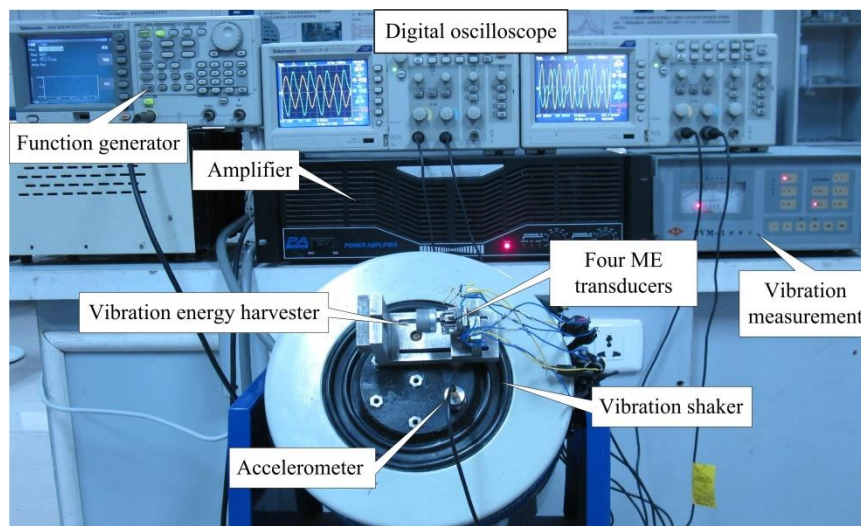


Fig. 7 Experimental setup

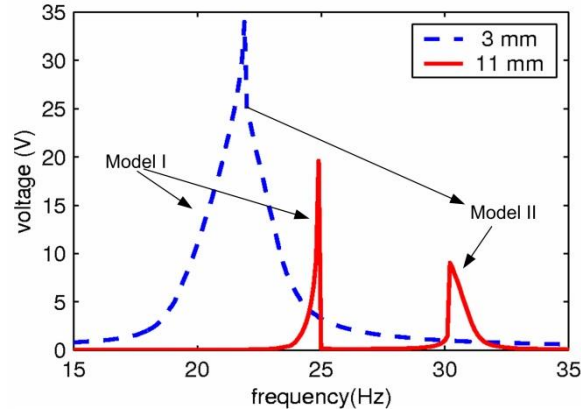


Fig. 8 Open-circuit voltages of the harvester with different ME initial positions

#### 4.2 Experimental results

In order to validate the influence of the initial position of the ME transducer on the output voltage, the open-circuit voltages of the harvester with one ME transducer placed on 3.0 mm and 11.0 mm are measured, respectively. Fig. 8 plots the frequency responses of the open-circuit voltages of the harvester at the excitation angle of  $45^\circ$  and acceleration of 0.6 g. As expected, the voltage output of the harvester with the ME transducer on 3.0 mm is higher than that on 11.0 mm. This is because the transducer can work in a better condition of the DC bias field at 3.0 mm than that at 11.0 mm, as analyzed in Section 3.1. Furthermore, as shown in Fig. 8, the vibration models I and II are both observed. And by nonlinear behavior of the magnetic force, hardening response and soft response of the rod are observed at models I and II, respectively. It is obvious that when the ME transducer is placed on 3.0 mm, the frequency response peaks of the vibration models I and II overlap together which allow the frequency response to be broadened. If the half peak voltage point is adopted as the criteria of the working bandwidth (Dai *et al.* 2012), in this case, the harvester shows a working bandwidth of 3.7 Hz, which is wider than that on 11.0 mm. It can be seen that from Fig. 8, the ME transducer and the magnetic circuit both contribute to the wide working bandwidth of the harvester.

Figs. 9(a)-9(c) plots the open-circuit voltages of the harvester with four ME transducers placed at 3.0 mm for different excitation angles of  $0^\circ$ ,  $45^\circ$  and  $90^\circ$  and acceleration of 0.6 g. As the angle was varied from  $0^\circ$  to  $90^\circ$ , the external vibrations at all angles can be harvested and converted to electricity. It is also noted that the output voltages of the four ME transducers are not the same. The output voltages of the ME transducers 1 and 2 are similar, and those voltages of ME transducers 3 and 4 are the same. For example in Fig. 9(a), at the mode I, the output voltages of the ME transducers 1 and 2 are similar and larger than those of the ME transducers 3 and 4, while at the mode II the output voltages of the ME transducers 3 and 4 become larger. These is because the two ME transducers 1 and 2 can induce similar and larger magnetic fields and variations to obtain higher output voltages at mode I, vice versa at mode II, as analyzed in Section 3.1.

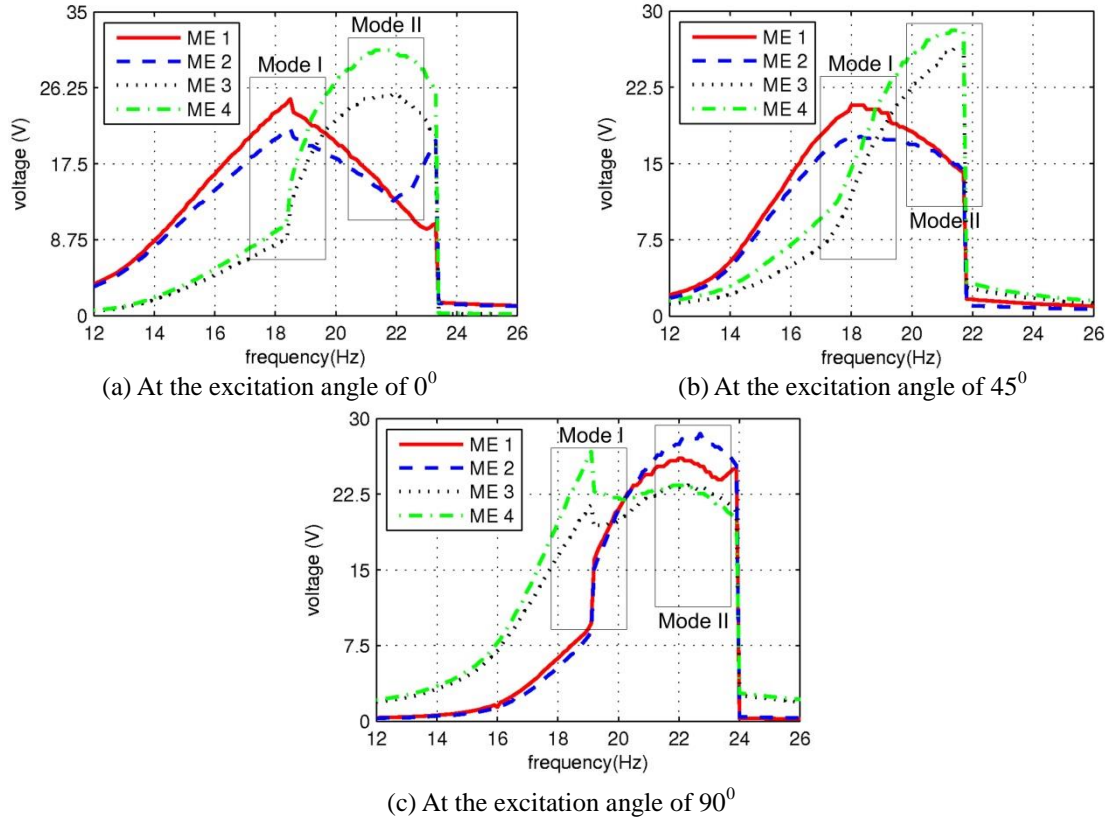


Fig. 9 Open-circuit voltages of the four ME transducers placed at 3.0 mm for different excitation angles

Fig.10 plots the open-circuit voltages of the harvester with four ME transducers placed on 11.0 mm at acceleration of 0.6 g. Similarly, the ME transducers 1 and 2 exhibit similar output characteristics, and the ME transducers 3 and 4 have same output voltages at these excitation angles. In addition, in Figs. 10(a) and 10(c) only one resonant mode is observed. It is seen that in Fig. 10(a), the peak voltages of ME transducers 1 and 2 respectively get to 30.0 V and 29.8 V at the excitation angle of  $0^{\circ}$ , which are larger than those of ME transducers 3 and 4. While in Fig. 10 (c) at the excitation angle of  $90^{\circ}$ , the peak voltages of ME transducers 1 and 2 become lower than those of ME transducers 3 and 4. In Fig. 10(b), the motion of the harvester shows two vibration modes with different resonant frequencies. At mode I with the resonant frequency of 25.5 Hz, ME transducers 1 and 2 have the peak voltages of 28.7 V and 28.0 V, respectively. At mode II with 27.5 Hz, the output voltages of ME transducers 3 and 4 get their maximum of 23.7 V and 21.5 V, respectively.

According to the measured open-circuit voltages in Figs. 9 and 10, the power can be estimated by the model in (Ferrari *et al.* 2010). The estimated optimal resistance of 5200 k $\Omega$  is used to calculate the output power of the harvester, as shown in Fig. 11. At all frequencies, the value of the power is the sum of powers of the four ME transducers. In Fig. 11(a) with four ME transducers placed at 3.0 mm, the corresponding frequency ranges of the two motion models I and II overlap

together to broaden the entire frequency response range of the harvester, which reach 5.5 Hz, 4.0 Hz, and 5.0 Hz at the excitation angles of  $0^\circ$ ,  $45^\circ$  and  $90^\circ$ , respectively. While in Fig. 11(b), the two resonance peaks are sharply separated and overlap slightly. The frequency bandwidths of the harvester are narrower than those in Fig. 11(a). This result confirms that the influence of the nonlinear and multi-model motion on the frequency range of the harvester. Although the maximum output power of the harvester with four ME transducers placed at 11.0 mm gets to 0.16 mW, which is larger than that of 0.13 mW at 3.0 mm,  $\sim 3.0$  mm is the optimal initial position to place the four ME transducers by taking into consideration the bandwidth and the output power.

## 5. Conclusions

In the harvester using multiple ME transducers, a circular cross-section cantilever rod is adopted to extract the ambient vibration energy with arbitrary directions. The influences of the initial position and multi-model motion on the electrical-output and the bandwidth of the harvester are investigated to achieve the optimal performances. The harvester can scavenge the vibration with arbitrary in-plane directions, and had a bandwidth of 5.5 Hz and sum of power of 0.13 mW at an acceleration of 0.6 g.

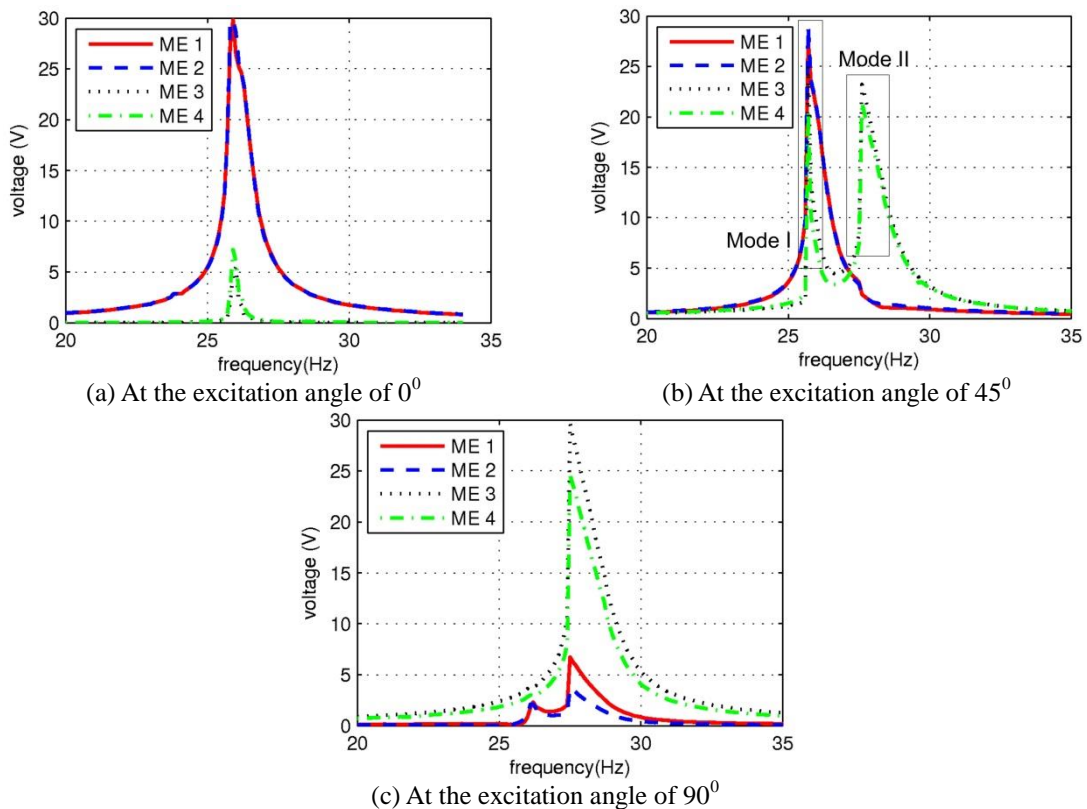


Fig. 10 Open-circuit voltages of the four ME transducers placed at 11.0 mm for different excitation angles

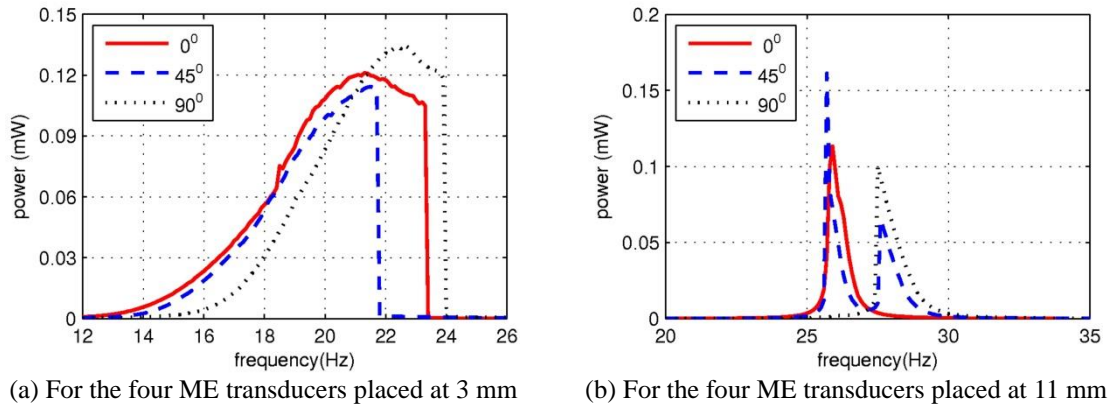


Fig.11 Output powers of the harvester

## Acknowledgments

This work was supported by the National Natural Science Foundation of China (No. 61174017), and by the National High Technology Research and Development Program of China (No. 2012AA040602).

## References

- Aladwani, A., Arafa, M., Aldraihem, O. and Baz, A. (2012), "Cantilevered piezoelectric energy harvester with a dynamic magnifier", *J. Vib. Acoust.*, **34**(3), 031004.
- Aladwani, A., Aldraihem, O. and Baz, A. (2013), "Single degree of freedom shear-mode piezoelectric energy harvester", *J. Vib. Acoust.*, **135**, 051011.
- Aldraihem, O. and Baz, A. (2011), "Energy harvester with a dynamic magnifier", *J. Intel. Mat. Syst. Str.*, **22**(6), 521-530.
- Arroyo, E. and Badel, A. (2011), "Electromagnetic vibration energy harvesting device optimization by synchronous energy extraction", *Sensor Actuat. A - Phys.*, **171**, 266-273.
- Bartsch, U., Gaspar, J. and Paul, O. (2009), "A 2-D electret-based resonant micro energy harvester", *Proceedings of the Technical Digest IEEE MEMS*, Sorrento, Italy, Jan. 25-29.
- Berdy, D.F., Jung, B., Rhoads, J.F. and Peroulis, D. (2012), "Wide-bandwidth, meandering vibration energy harvester with distributed circuit board inertial mass", *Sensor Actuat. A - Phys.*, **188**, 148-157.
- Casciati, S., Faravelli, L. and Chen, Z. (2012), "Energy harvesting and power management of wireless sensors for structural control applications in civil engineering", *Smart Struct. Syst.*, **10** (3), 299-312.
- Chen, J.D., Chen, D., Yuan, T. and Chen, X. (2012), "A multi-frequency sandwich type electromagnetic vibration energy harvester", *Appl. Phys. Lett.*, **100**, 213509.
- Chen, J., Zhu, G., Yang, W., Jing, Q., Bai, P., Yang, Y., Hou, T.C. and Wang, Z.L. (2013), "Harmonic-Resonator-Based Triboelectric Nanogenerator as a Sustainable Power Source and a Self-Powered Active Vibration Sensor", *Adv. Mater.* doi:10.1002.
- Dai, X., Miao, X., Sui, L., Zhou, H., Zhao, X. and Ding, G. (2012), "Tuning of nonlinear vibration via topology variation and its application in energy harvesting", *Appl. Phys. Lett.*, **100**, 031902.
- Erturk, A. and Inman, D.J. (2011), "Broadband piezoelectric power generation on high-energy orbits of the bistable Duffing oscillator with electromechanical coupling", *J. Sound Vib.*, **330**, 2339-2353.
- Ferrari, M., Ferrari, V., Guizzetti, M., Andò, B., Baglio, S. and Trigona, C. (2010), "Improved energy

- harvesting from wideband vibrations by nonlinear piezoelectric converters”, *Sensor Actuat. A-Phys.*, **162**, 425-431.
- Guan, X.C., Huang, Y.H., Li, H. and Ou, J.P. (2012), “Adaptive MR damper cable control system based on piezoelectric power harvesting”, *Smart Struct. Syst.*, **10**(1), 33-46.
- Jung, H., Kim, I.H. and Koo, J.H. (2011), “A multi-functional cable-damper system for vibration mitigation, tension estimation and energy harvesting”, *Smart Struct. Syst.*, **7**(5), 379-392.
- Kim, S. and Chun, K. (2012), “2D Vibration based MEMS Energy Harvester”, *Proceedings of the International Conference on Renewable Energies and Power Quality*, Santiago de Compostela, Spain, 28th to 30th March.
- Kim, S. and Na, U. (2013), “Energy harvesting techniques for remote corrosion monitoring systems”, *Smart Struct. Syst.*, **11**(5), 555-567.
- Moss, S., Barry, A., Powlesland, I., Galea, S. and Carman, G. P. (2011), “A broadband vibro-impacting power harvester with symmetrical piezoelectric bimorph-stops”, *Smart Mater. Struct.*, **20**, 045013.
- Moss, S.D., McLeod, J.E., Powlesland, I.G. and Galea, S.C. (2012), “A bi-axial magnetoelectric vibration energy harvester”, *Sensor Actuat. A - Phys.*, **175**, 165-168.
- Nguyen, D.S., Halvorsen, E., Jensen, G.U. and Vogl, A. (2010), “Fabrication and characterization of a wideband MEMS energy harvester utilizing nonlinear springs”, *J. Micromech. Microeng.*, **20**, 125009.
- Ramlan, R., Brennan, M.J., Mace, B.R. and Kovacic, I. (2010), “Potential benefits of a non-linear stiffness in an energy harvesting device”, *Nonlinear Dynam.*, **59**, 545-558.
- Stanton, S.C., McGehee, C.C. and Mann, B.P. (2009), “Reversible hysteresis for broadband magnetopiezoelectric energy harvesting”, *Appl. Phys. Lett.*, **95**, 174103.s.
- Tvedt, L.G.W., Nguyen, D.S. and Halvorsen, E. (2010), “Nonlinear behavior of an electrostatic energy harvester under wide- and narrowband excitation”, *J. Microelectromech. S.*, **19** (2), 305-316.
- Wang, L. and Yuan, F.G. (2008), “Vibration energy harvesting by magnetostrictive material”, *Smart Mater. Struct.*, **17**, 045009.
- Yang, J., Wen, Y.M. and Li, P. (2011), “Magnetoelectric energy harvesting from vibrations of multiple frequencies”, *J. Intel. Mat. Syst. Str.*, **22**, 1631-1639.
- Yang, J., Wen, Y.M., Li, P. and Dai, X.Z. (2011), “A magnetoelectric, broadband vibration-powered generator for intelligent sensor systems”, *Sensor Actuat. A - Phys.*, **168**, 358-364.
- Zhang, Y. and Zhu, B.H. (2012), “Analysis and simulation of multi-mode piezoelectric energy harvesters”, *Smart Struct. Syst.*, **9**(6), 549.
- Zhu, D.B., Beeby, S.P., Tudor, M.J. and Harris, N.R. (2011), “A credit card sized self powered smart sensor node”, *Sensor Actuat. A - Phys.*, **169**, 317-325.
- Zhu, Y., Moheimani, S.O.R. and Yuce, M.R. (2011), “A 2-DOF MEMS Ultrasonic Energy Harvester”, *IEEE Sens. J.*, **11**(1), 155-161.